Deexcitation rates for $He^+(2S)$ in collision with atoms and molecules*

M. H. Prior and E. C. Wang
Department of Physics and Lawrence Berkeley Laboratory, University of California, Berkeley, California 94720
(Received 30 October 1973)

We have studied the deexcitation of He^+ ions in the $2S$ metastable state by collision with eleven different target gases. These include noble gases, symmetric linear molecules, water, and ammonia. From our data we extract velocity-averaged total deexcitation-rate constants $\langle \sigma v \rangle$ ranging from $1.65(17) \times 10^{-9}$ to $20.9(21) \times 10^{-9}$ $cm^3 sec^{-1}$ for helium and ammonia, respectively. In all cases the mean energy of the He^+ ions was $\simeq 0.23$ eV and the target gases had a 300 °K Maxwell-Boltzmann distribution of velocities. The results are consistent with collision-induced Lyman-α emission being a prominent deexcitation mechanism.

I. INTRODUCTION

In the past a fair amount of experimental and theoretical effort has been expended on the problem of the deexcitation of hydrogen atoms in the metastable $2S$ state by near thermal-energy collisions with atoms and molecules. Both experimentally and theoretically the problem seems to be tractable, a circumstance which adds the usual synergistic term to the rate of progress. Most recently there has been the experimental work of Kass and Williams,[1] Czuchlewski and Ryan,[2] and Comes and Wenning.[3] Preceding these was the pioneering work of Fite and co-workers.[4,5] On the theoretical side recent papers by Byron and Gersten[6,7] and Slocomb, Miller, and Schaeffer[8] are notable.

In this work we report experimental studies of the nearly analogous problem of collisional deexcitation of $He^+(2S)$. Exact analogy fails because the positive charge of the ion plays an important role, but the broad picture of the deexcitation process remains.

Briefly, the current understanding is that the transient electric field seen by the metastable projectile during its passage near a target atom or molecule mixes the $2S$ and $2P$ states via the Stark interaction, leaving it with a finite probability of being in one of the $2P$ states after the collision. Since the lifetime of the $2P$ state is very short ($\simeq 10^{-9}$ sec for H, 10^{-10} sec for He^+), the projectile returns to the ground ($1S$) state emitting a Lyman-α photon ($\lambda \simeq 300$ Å for He^+) long before it can meet another target.

The interaction potential responsible for the transient field will depend, of course, upon the nature of the target and the charge of the hydrogenlike metastable projectile. In the case of $H(2S)$ in collision with a spherical target (e.g., a noble-gas atom) the interaction is, roughly,[8] that of the transient $(2S+2P)$ quadrupole moment interacting with the electric field produced by the dipole induced in the target by the $(2S+2P)$ dipole moment. Thus it is proportional to the polarizability of the target and has a r^{-7} dependence on the separation r. In the case of molecular collisions the interaction is generally of longer range being via the electric multipole field surrounding the target. Thus for polar molecules the interaction potential is proportional to the molecular dipole moment and falls as r^{-3}. When the metastable projectile is charged, as with $He^+(2S)$, one has, in addition, to consider the interaction induced by the Coulomb field. This yields a potential proportional to the target dipole polarizability and varying as r^{-4}.

The deexcitation rates measured in this work are total rates, i.e., they are the sum of the rates for all processes leading to deexcitation of $He^+(2S)$. Since $He^+(2S)$ possesses 40.8 eV of excitation energy, a host of deexcitation mechanisms are possible. The most probable are induced Lyman-α decay as described above and nonradiative deexcitation with simultaneous ionization of the target (Penning ionization), i.e., the process,

$$He^+(2S) + X \rightarrow He^+(1S) + X^+ + e^- .$$

In addition when the target is a molecule, a number of ion-neutral reactions are possible. Many of these would lead to dissociation and ionization of the target molecule. Very little, if any, information is available for rates of such processes when the projectile is a highly excited metastable ion such as $He^+(2S)$. We believe, however, that regardless of the target, the induced Lyman-α rate accounts for more than half of the total deexcitation rate. We present some experimental evidence which shows that for collisions with He, it is a prominent process.

II. EXPERIMENTAL METHOD

The present work is an outgrowth of an experiment[9] carried out to measure the free lifetime τ_0

of $He^+(2S)$. The result of that experiment was $\tau_0 = 1.922(82)$ msec. which is in agreement with the theoretical value[10] of 1.899 msec. The same apparatus was used in these experiments with some modifications, principally to allow absolute measurement of target-gas-pressure increments.

The unperturbed $2S$ state decays by emission of two electric dipole photons[11] with energies such that $h\nu_1 + h\nu_2 = 40.8$ eV. The single photon distribution is then a continuous one with a short-wavelength cutoff at $\lambda_{min} = 304$ Å and extending to infinite wavelength. The distribution[12] rises rapidly from λ_{min} to a peak at $\simeq 350$ Å after which the intensity falls off roughly as $\exp[-(\lambda - 350)/430]$.

The method used is based on the following simple ideas. If one has a quantity N of $He^+(2S)$ ions confined to some volume containing a density n_{He} of helium atoms and n of target atoms or molecules then the usual simple first-order differential equation applies to the variation of N with time:

$$dN/dt = -N(A + \sigma_{He} v n_{He} + \sigma v n), \quad (1)$$

where $A = 1/\tau_0$, σ_{He} and σ are total deexcitation cross sections for collisions with helium and the target of study, and v is the relative collision velocity (here assumed to be the same for each type of collision). The solution is

$$N = N(t=0)e^{-t/\tau}, \quad (2)$$

where

$$1/\tau = A + \sigma_{He} v n_{He} + \sigma v n. \quad (3)$$

Thus, if one holds v and n_{He} constant, a plot of the measured quantities $1/\tau$ vs n should yield a straight line whose slope is the product σv. If one has a unique and known value of v then one could extract σ. In these experiments, however, one has present a distribution of relative velocities so that the quantity derived from such a plot is $R = \langle \sigma v \rangle$, the velocity-averaged product. It turns out that the distribution of v present in the measurements reported here is, to a good approximation, independent of the target, and hence trends in R reflect trends in σ.

The technique used to measure $1/\tau$ vs n is as follows. A quantity ($\simeq 10^2$) of $He^+(2S)$ ions are created by pulsed electron impact on He gas ($p_{He} \simeq 10^{-6}$ Torr) at time $t = 0$. The ions are confined inside an electromagnetic ion trap for a period of 4 msec. During this storage time the $He^+(2S)$ ions make collisions with the He gas and with the target gas at a pressure p; single decay photons are detected by windowless electron multipliers and the resulting pulses are stored versus time in 100 channels of a multichannel scalar (40 μsec/channel). At the end of the storage period, all ions are dumped from the trap and a new cycle is begun. Many fill-store-dump cycles are repeated until a decay curve is accumulated with sufficiently small statistical fluctuations to allow determination of a value for τ. This may take from 15 min to 2 h depending on the experimental conditions. The whole process is repeated for different values of p to determine the line $1/\tau$ vs n ($n = p/kT$).

Figure 1 shows the ion trap and photon detectors. The ion trap is a closed cylinder (radius $\simeq 15$ cm, length $\simeq 30$ cm) whose ends are maintained at a positive potential with respect to the body; the potential difference during these measurements was 2.0 V. A magnetic field of $\simeq 60$ G was applied coaxial with the cylinder by means of coils external to the vacuum enclosure. The electrostatic field confines ion motion along the magnetic field, while the magnetic field limits motion perpendicular to the trap axis.

The trap is constructed primarily from oxygen-free high-conductivity copper, stainless steel,

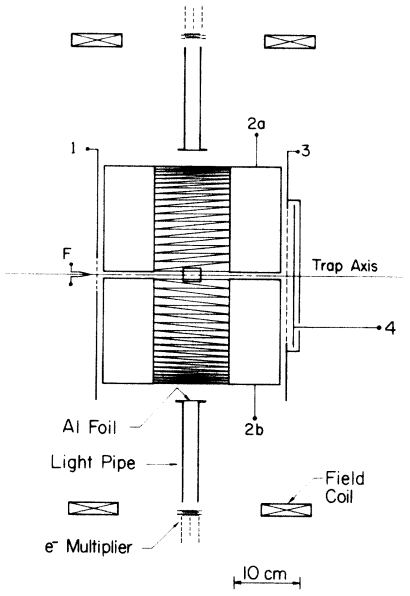

FIG. 1. Sketch of the ion trap and photon detectors. The magnetic field is along the trap axis. The half cylinders $2a$ and $2b$ are maintained negative with respect to electrodes 1 and 3 during the storage period. The hot filament F is pulsed negative to accelerate electrons into the trap for creation of the He ions. The zig-zag pattern is a web of thin copper wires to give high transparency for the decay photons, while maintaining the cylindrical electrode geometry. The rectangular shape in the center of the figure represents the end of the microwave horn located outside the cylinder. Power radiated from this horn drives the $2S$-$2P_{1/2}$ transition.

and alumina insulators; the vacuum enclosure is entirely of stainless steel. After bake out, pressures of $< 2\times10^{-9}$ Torr have been achieved, however during these measurements the background pressure was more typically $\simeq 8\times10^{-8}$ Torr. Helium and target gases are admitted to the chamber containing the trap via separate micrometer controlled variable leak valves. These in turn are connected to separate gas handling systems. The micrometer valves allowed sensitive control of p_{He} and p during the measurements. A quadrupole residual-gas analyzer is attached to the chamber and is used to monitor the constituents of the background gas and the purity of the admitted target gas.

Helium ions are created inside the trap by impact from an electron pulse accelerated along the axis. Typically the electron pulse is 4.0 μA, lasts 0.75 msec, and has an energy of 225 eV. At a helium pressure of 8×10^{-6} Torr this yields about 10^6 ions, of which about 10^3 can be expected to be in the $2S$ metastable state. At the end of a storage period the trap potentials are altered so that ions are dumped onto a collecting plate (electrode 4 in Fig. 1); this allows monitoring of the number of stored ions via the size of the resulting positive-current pulse which was displayed on an oscilloscope and averaged via a boxcar integrator. The electron pulse also appears on this electrode during the trap fill time. Of course, background and target-gas ions are created by the electron pulse in addition to He ions. However, except for the case when the target gas is H_2, these ions have too small a charge-to-mass ratio to be confined and in a fraction of a millisecond leave the trap volume—only the He ions remain. The heavy ions do compete for space in the trap, however, during the fill period and the transient period during which they leak from the trap, and, since the trap has a finite capacity for confined charge ($\simeq 10^7$ positive charges), they affect the number of He ions which are ultimately stored for a given electron pulse. One observes a decrease in the number of stored He ions when one holds the electron pulse and p_{He} constant and increases p. This effect is one of the factors limiting the range over which p may be varied for a given target.

As is indicated in Fig. 1, the cylindrical portion of the trap is made up of two half-cylinders $2a$ and $2b$; this allows application of an alternating potential between them (while maintaining a common dc potential) which can excite resonant motion of the stored ions at their cyclotron frequency. At resonance the ions gain energy from the ac field until they strike the electrodes or chamber walls; thus one observes a drop in the ion dump-pulse amplitude when the applied frequency is in resonance. In addition to the cyclotron resonance, one observes resonance at the frequency of motion along the trap axis (z motion) and at the magnetron frequency (frequency of drift of the cyclotron orbit center about the trap axis). To excite the z-motion resonance it is more convenient to apply the ac potential between electrodes 1 and $2a, 2b$ connected together.

Observation of the z-motion resonance allows determination of the effective harmonic potential-well depth, W, along the z axis. Thus $W = kz_m^2/2q$, where $k = m(2\pi f_z)^2$ and z_m is the maximum amplitude of z motion, q the ion's charge, m its mass, and f_z the z-motion frequency. For helium ions with trap potentials as described above, f_z was measured to be $f_z = 7.98(50)$ kHz. With $z_m = 12.9$ cm one obtains $W = 0.87(11)$ eV.

The photon detectors are two EMI 9642/2 18-stage CuBe Venetian-blind electron multipliers. To prevent metastable helium atoms ($2\,^3S_1$ and $2\,^1S_0$) as well as metastable background and target-gas atoms or molecules from reaching the multipliers, their view of the storage volume is covered by aluminum foils 18 mm in diameter and 800 Å thick. The foils have a transmission varying between 10% and 70% over the region 200–700 Å. The Al-foil, CuBe-multiplier combination responds to $\simeq 2\%$ of the radiation over the range 300–500 Å which strikes the Al foil. The two light pipes are Pyrex tubes coated internally with a 1000-Å thickness of gold; they enhance the count rate by about a factor of 4 over the case with no light pipes.

To establish that the observed decay is that from $He^+(2S)$, microwave power ($\simeq 150$ mW) at the Lamb-shift frequency (14.045 GHz) is broadcast into the trap volume via a wave-guide horn. This converts a large fraction (more than 80%) of the $2S$ ions to the $2P_{1/2}$ state from which they immediately decay, destroying the $2S$ decay curve. The microwave power is generated by a Varian X-12 klystron and may be on-off modulated via a pin-diode switch under control of the data-collection logic system.

One typical data cycle consists of the following sequence: a 0.75-msec fill period during which the electron pulse is on, a delay period of 0.8 msec during which the microwave power may or may not be applied, a storage period of 4 msec during which counts from the multipliers are accumulated versus time in 100 channels of the memory unit, and a 75-μsec ion-dump period. Data are stored in two separate 100-channel blocks of the memory unit corresponding to the microwave power being on or off during the delay period. Usually the microwave power is switched on or

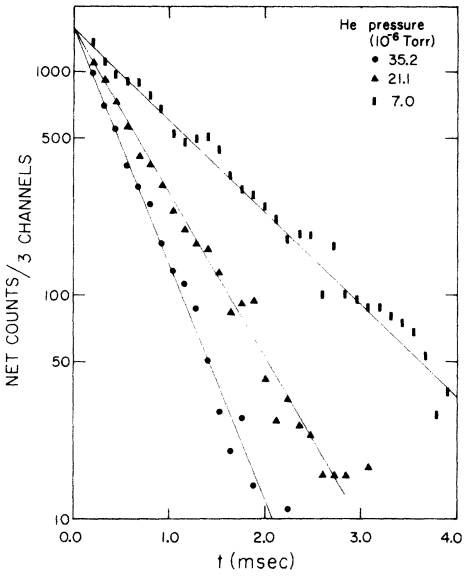

FIG. 2. Representative $He^+(2S)$ decay curves for three different pressures of He. The lines are computer fits. The curves have been adjusted slightly vertically so that the lines meet at $t=0$. The ordinate is correctly scaled for the data at 7.0×10^{-6} Torr.

off every 5000 data cycles. The time base for the system is derived from a 100-kHz crystal oscillator.

The pressure p was measured by a nude Bayard-Alpert ionization gauge calibrated against a Datametrics model 1023 capacitance manometer. For most of the targets, p ranged from zero to $\simeq 3.0\times10^{-6}$ Torr. The highest sensitivity of the capacitance manometer is 10^{-4} Torr full scale, thus the ion gauge was calibrated at pressures $\simeq 10$ times those used in taking the deexcitation data; this procedure is valid due to the highly

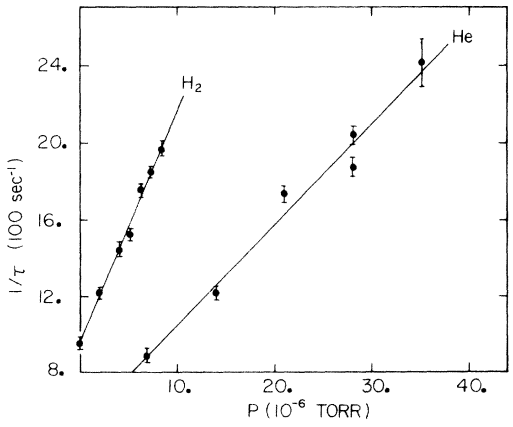

FIG. 3. $1/\tau$ vs pressure plots for $He^+(2S)$ collisions with H_2 and He. The lines are least-squares computer fits.

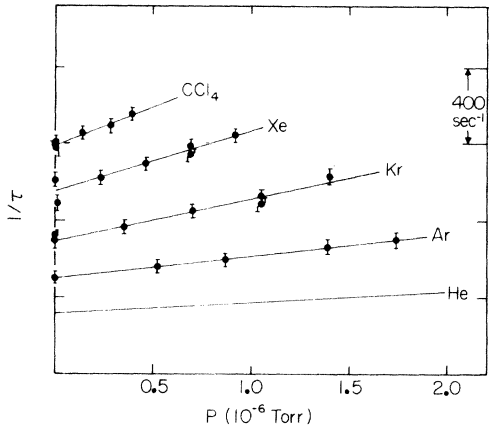

FIG. 4. $1/\tau$ vs pressure plots for $He^+(2S)$ collisions with He, Ar, Kr, Xe, and CCl_4. The curves have been separated vertically for clarity since the slopes are the quantities of interest. The lines are least-squares computer fits. The line for He is that shown in Fig. 3.

linear response of the ion gauge and the fact that one requires only the slope of the ion-gauge response versus absolute pressure. Put another way, to measure R one need only determine $\Delta(1/\tau)/\Delta n$ which in turn requires only measurement of absolute-pressure increments Δp. Typical calibrations would consist of setting p to ten different values ranging from $(1.0 \text{ to } 10.0)\times10^{-5}$

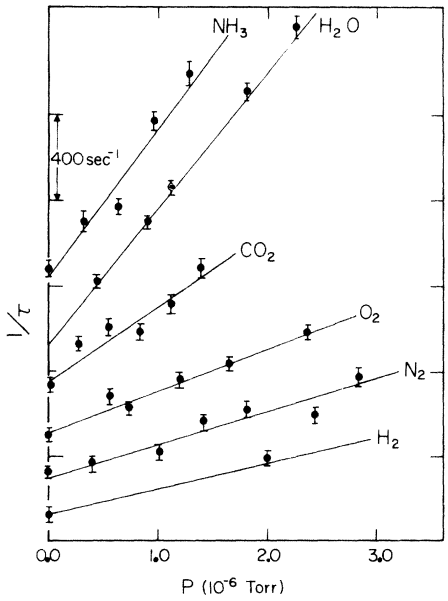

FIG. 5. $1/\tau$ vs pressure plots for $He^+(2S)$ collisions with H_2, N_2, O_2, CO_2, H_2O, and NH_3. The curves have been separated vertically for clarity since the slopes are the quantities of interest. The lines are least-squares computer fits. The line and points for H_2 are the low-pressure end of the plot shown in Fig. 3.

Torr as read by the ion gauge and noting the corresponding capacitance manometer readings. The data were fitted by the method of least squares to the straight-line form,

$$p = Mp_I + C , \quad (4)$$

where p_I is the ion-gauge reading and M and C were varied to make the fit. For each determination of R, requiring about one day's data collection, there were made at least one and often two calibrations of the ion gauge. We found that generally the calibration constant M remained unchanged from day to day within a few percent and that the statistical error of the fitted M for a given set of calibration data was usually much less than 5%.

Figure 2 shows decay data for $He^+(2S)$ at three different He-gas pressures. This data was used to determine R_{He}. The data are the difference between counts accumulated with microwave power on and off. Each point is the sum of three 40-μsec channels. About 1-h data-collection time was required to obtain each curve. The lines through the data are least-squares computer fits to the function $Ae^{-t/\tau}+B$, where A, B, and τ are varied to make the fit. The constant background-term B was always consistent with zero. Similar sets of curves were obtained for each of the target gases studied, although the pressure range for most was $\simeq$10 times less due to the drop off of the number of stored He ions with increasing p as mentioned previously.

Figures 3–5 show $1/\tau$ vs p data representative of that used to determine R values for all of the targets studied. Several such curves were obtained for each target and the results were determined from an average of the slopes measured by computer fit to the data.

III. RESULTS

Table I contains the results of our measurements. The errors are the larger of one standard deviation of the mean of each set of measurements for a given target or 10% of the mean. In addition to the values of R we have included the ratios R/R_{He}. This quantity is equal to the ratio σ/σ_{He} if the cross sections have the same dependence on relative velocity and the relative-velocity distribution is the same for both targets. The latter is a good approximation since we estimate (see Sec. IV) the mean energy of the stored He^+ ions to be $\simeq 0.23$ eV, whereas the mean energy of the targets is 300 °K thermal, $\simeq 0.039$ eV. One can then regard the distribution of relative velocities to be essentially equal to the distribution of He^+-ion velocities which was the same for all the measurements. The greatest error would occur for the case of H_2 where the correction would increase the mean relative velocity by about 6%. One does not expect, however, that the cross sections have the same velocity dependences except among the group including the noble gases and CCl_4.

We have also included in Table I effective cross sections, σ_{eff}, obtained from R by dividing by the velocity $v = 3.3\times10^5$ cm/sec equivalent to a He ion of 0.23-eV energy. These are intended only to indicate the range and size of the deexcitation cross sections for $He^+(2S)$ at this energy.

An essentially exponential decay of ground-state He^+ ions versus storage time was noted during these measurements; its decay time varied linearly with pressure p and hence is consistent with the existence of some single-collision loss mechanism. In the case of noble-gas targets the rate constant for this process was always quite small, $\leq 5\%$ of R. We hypothesize that possibly, due to the departure of the trap geometry from a perfect quadrupole shape, certain regions of phase space can lead to ion loss. Such a loss mechanism would be proportional to the ion-atom momentum transfer cross section and could conceivably explain the effect.

In the case of molecular targets the loss rate of ground-state He^+ ions was observed to be considerably larger. In particular, N_2, O_2, and CO_2 were studied. We observed loss-rate constants of 1.4(3), 1.1(3), and 1.5(4) in units of 10^{-9} cm^3 sec^{-1}, respectively, for these targets. The rates for N_2 and O_2 are in agreement with reaction rates measured by Ferguson *et al.*[13] and Sayers and Smith[14] for the processes,

$$He^+ + N_2 \rightarrow He + N^+ + N + 0.3 \text{ eV},$$

TABLE I. Results of $He^+(2S)$ deexcitation rate measurements.

Target	R (10^{-9} cm^3 sec^{-1})	R/R_{He}	σ_{eff} [a] (Å^2)
He	1.65(17)	1.00	52.0
Ar	4.99(65)	3.02(50)	156.0
Kr	6.3(10)	3.82(72)	199.0
Xe	8.7(14)	5.24(55)	273.0
CCl_4	13.3(13)	8.1(12)	420.0
H_2	3.68(37)	2.23(32)	116.0
N_2	5.51(55)	3.34(48)	174.0
O_2	6.07(61)	3.68(53)	191.0
CO_2	11.3(16)	6.9(12)	360.0
H_2O	18.5(19)	11.2(16)	585.0
NH_3	20.9(21)	12.6(18)	659.0

[a] $\sigma_{eff} = R/v$, where $v = 3.3\times10^5$ cm/sec.

and

$$He^+ + O_2 \rightarrow He + O^+ + O + 5.9 \text{ eV}.$$

These authors studied the above reactions in He afterglows. Any reactions similar to the above and involving $He^+(2S)$ ions would of course be included in the measured values of R. We assume that the small-loss-rate mechanism ($\leq 5\%$ of R) noted for ground-state ions on noble gases, if present for $He^+(2S)$ collisions with these and other targets, is no larger and the quoted values of R contain no correction for it.

We point out that for a perfect trap geometry one might expect some ion loss due to elastic collisions which allow a "random walk" of the ion orbit across the magnetic field or leakage along the trap axis. The latter collisions would be most probable while the ion is at one extreme of its z trajectory. Both of these processes would require multiple collisions, on the average, to cause loss of an ion because of the cross-sectional size of the orbit ($\simeq 5$ cm) in comparison to the trap diameter, and the small energy transfer available ($\simeq 0.025$ eV) per collision. A multiple-collision loss process would imply a nonexponential decay curve if it were present to any significant degree as well as a nonlinear relationship between any fitted $1/\tau$ and p. Neither of these appear in our data to well within the limits indicated by the quoted errors.

In addition to measuring R values as described above, we did some experiments to determine whether or not the collision-induced Lyman-α decay is a prominent decay mechanism for collisions with helium atoms. This was done by studying the variation of the normalized metastable decay rate, at a fixed time after creation of the ions, versus helium pressure.

The differential equation for decay of the $He^+(2S)$ population N may be rewritten as

$$dN/dt = S_r + S_{nr}, \tag{5}$$

where S_r and S_{nr} are rates for radiative and nonradiative processes, respectively. For the case of impact on helium atoms one has

$$S_r = -N(A + \sigma_r v n), \tag{6}$$

$$S_{nr} = -N\sigma_{nr} v n, \tag{7}$$

where A is the free-ion decay rate, $n = n_{He}$, and σ_r σ_{nr} are cross sections for radiative and nonradiative deexcitation. The normalized rate of photon emission, $G = S_r/N(t=0)$, at time t after creation of $2S$ ions at $t=0$ is given by

$$G = (A + \sigma_r v n)\exp[-t(A + \sigma_r v n + \sigma_{nr} v n)]. \tag{8}$$

The actual measured normalized rates F, would be given by

$$F = K(A + \xi D p)e^{-t(A + Dp)}, \tag{9}$$

where

$$D = (\sigma_r v + \sigma_{nr} v)/kT \tag{10}$$

and

$$\xi = \eta\sigma_r v/(\sigma_r v + \sigma_{nr} v). \tag{11}$$

K is a proportionality constant involving detector geometry and efficiency factors, $p = p_{He}$, and η is the relative efficiency of the detectors for collision-induced versus free-decay photons. η is most probably not unity since each free decay produces two photons with a continuous single-photon spectrum whereas collision-produced photons are produced one per decay and are at the Lyman-α wavelength 304 Å. The quantity ξ, if $\eta = 1.0$, is a measure of the fraction of deexcitation collisions which produce a photon. In the above, the products $\sigma_r v$ and $\sigma_{nr} v$ may be replaced by velocity-averaged products.

We have measured F vs p at $t = 1$ msec in an attempt to learn something about the size of ξ. Figure 6 shows a plot of the data. The two curves are F vs p for $\xi = 0.0$ and 1.0 using the measured value of $D = R_{He}/kT$, $T = 300\,^\circ$K, and adjusting K by eye to give the best fit for $\xi = 1.0$. The data is consistent with $0.5 \lesssim \xi \lesssim 1.5$. It is reasonable to assume that $0 < \eta \lesssim 2$. Thus for collisions of $He^+(2S)$ on helium atoms we conclude that at least 25% of the deexcitation collisions produce photons.

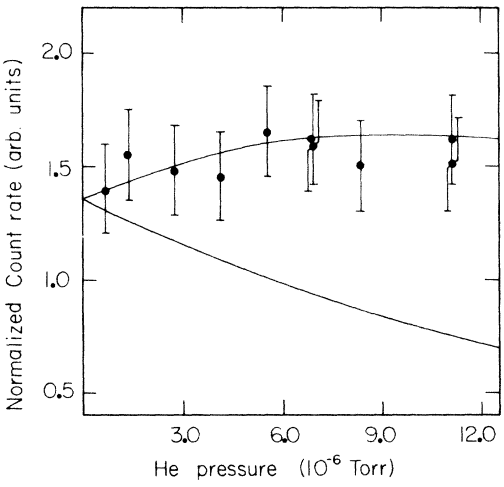

FIG. 6. Plot of the normalized count rate for $He^+(2S)$ in collision with He at $t = 1$ msec after creation of the ions vs He pressure. The upper and lower curves are plots of the function F for $\xi = 1.0$ and 0.0, respectively. The data indicates that at least 25% of the collisions produce countable photons.

IV. DISCUSSION

In the following we discuss our results primarily in terms of the mechanism of induced Lyman-α decay. This is done because it is most probably the predominant deexcitation mode and to some extent one can apply the theory already developed for H(2S) deexcitation to the $He^+(2S)$ collisions studied here.

A. Spherical targets

If one takes as the interaction potential between the $He^+(2S)$ ion and a target with polarizability α, the form[15]

$$U(r) = -e\alpha^2/2r^4 , \tag{12}$$

with r the internuclear separation and e the electronic charge, then a simple dimensional argument shows that the induced Lyman-α decay-rate constant should be given by

$$R = C(\alpha\mu v)^{1/2} , \tag{13}$$

where C is a constant and μ is the matrix element $|\langle 2P|z_e|2S\rangle|$, z_e being the z coordinate of the He^+ electron. (The "natural" z axis is along the internuclear axis.) We have calculated R using the potential above and straight-line trajectories using the sudden approximation.[16] The sudden approximation is applicable because of the short duration of the collision, $\simeq 10^{-13}$ sec, in comparison to the $2S-2P_{1/2}$, $2P_{3/2}$ fine-structure periods, $\simeq 10^{-10}$, $\simeq 10^{-11}$ sec. The small-impact-parameter cutoff is the usual one, i.e., that value B_0 such that $P(B_0)$ (the probability of the ion being in one of the $2P$ states after collision) is equal to unity. For impact parameters less than B_0, P oscillates rapidly between zero and unity and may be replaced by its average value of $\frac{1}{2}$. The cross section is then

$$\sigma = 0.5\pi B_0^2 + 2\pi \int_{B_0}^{\infty} bP(b)\,db . \tag{14}$$

The result of the calculation is

$$R = 4.28(e^2\alpha\mu v/\hbar)^{1/2} . \tag{15}$$

For He^+, $\mu = 1.5a_0$, with a_0 being the Bohr radius.

In order to compare values obtained from Eq. (15) with our measurements we need a value for $\langle v^{1/2}\rangle$, the velocity-averaged square root, appropriate to the distribution of metastable ion velocities in the trap. This distribution may be thought of as arising from three sources: (i) the uniform distribution of ion potential energies along the z axis during the electron pulse, (ii) the thermal distribution of the He atoms before ionization, and (iii) the distribution of $He^+(2S)$ recoil velocities after electron impact. The initial metastable-ion velocity distribution (i.e., that present immediately after the electron pulse) is the net effect of the above. It will be nonisotropic and non-Maxwellian because of the contributions of (i) and (iii). Furthermore the distribution will evolve in time toward an equilibrium one at a rate dependent on the strength of several relaxation mechanisms.

The velocity distribution produced by (i) alone would be one of constant amplitude for $-v_m < v_z < v_m$, $v_m = 2\pi f_z z_m = 6.5\times 10^5$ cm/sec, and zero elsewhere with no x or y components. Source (ii) of course is the Maxwell distribution with a most probable velocity of $v_t = 1.11\times 10^5$ cm/sec (300 °K). Distribution (iii) is not known. One can estimate the average recoil velocity following a procedure adopted by Lipworth and Novick[17] which is based on a treatment of hydrogen electron-impact ionization. One assumes that the average ion-recoil momentum is equal in magnitude to the average momentum of the ejected electron. The latter is taken to correspond to that of a He K-shell electron velocity of $Z_{\text{eff}}c/137$. With $Z_{\text{eff}} = 1.69$ one has $v_r = 0.51\times 10^5$ cm/sec.

It is not possible to construct the net initial distribution due to our ignorance of (iii), however from the relative sizes of v_m, v_t, and v_r we expect (i) to dominate with small x and y components added by (ii) and (iii) and a rounding of the distribution of z velocities starting at $|v_z| \gtrsim v_m'$, where $v_m' = v_m - (v_t^2 + v_r^2)^{1/2} = 5.3\times 10^5$ cm/sec. We take then as an estimate of the rms velocity for the initial distribution, $\langle v^2\rangle^{1/2} \simeq (v_m'^2 + v_t^2 + v_r^2)^{1/2} = 3.3\times 10^5$ cm/sec.

The initial distribution will evolve in time because of (i) elastic ion-ion collisions, (ii) elastic ion-neutral collisions, and (iii) symmetric charge exchange with He atoms [i.e., $He^+(2S) + He \rightarrow He + He^+(2S)$].

The collision interval t_I for process (i) can be estimated by a uniform plasma approximation given by Spitzer[18] which yields

$$t_I = 0.0557 M^{1/2}(3kT)^{3/2}e^{-4}(n_I \ln\Lambda)^{-1} , \tag{16}$$

for ions of mass M, charge e, density n_I, and an effective temperature T. Λ is the ratio of the cutoff distance for Coulomb interaction of an ion with its neighbors to the distance of closest approach. The cutoff is $\simeq z_m$ and the closest approach is $\simeq n_{\max}^{-1/3}$ with $n_{\max}$ the maximum ion density stored. We have $\ln\Lambda \simeq 10$, and taking $3kT \simeq 0.46$ eV, one has $t_I \simeq 1.6$ sec for $n_I = 10^5$ cm^{-3}.

Using the theory of orbiting collisions in an inverse fourth-power polarization potential as developed by Eliason and Hirschfelder,[19] one calculates a collision interval t_A for momentum trans-

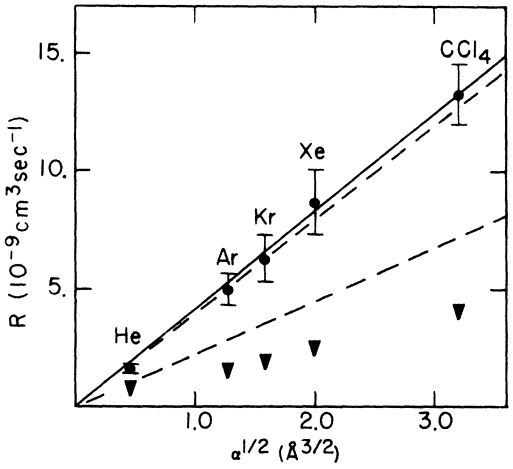

FIG. 7. Plot of experimental values of the $He^+(2S)$ total deexcitation rate vs the square root of the polarizability of the targets He, Ar, Kr, Xe, and CCl_4. The dashed lines are the results of the sudden-approximation calculation, Eq. (15), using the extreme estimates for $\langle v^{1/2}\rangle$. The solid line is a least-squares straight-line fit to the data. The triangles are momentum transfer rates.

fer appropriate to process (ii) from $t_A=(R_A n_A)^{-1}$, with n_A the density of neutrals and

$$R_A = 6.94e(\alpha/M_r)^{1/2}, \tag{17}$$

where M_r is the reduced mass of the collision partners and α is the polarizability of the neutral. For $\alpha = 4.0$ Å^3, $n_A = 10^{11}$ cm^{-3}, and $M_r = 4$ amu, one has $t_A = 12$ msec.

For process (iii) we estimate that the symmetric charge-exchange cross section at a velocity of 3.3×10^5 cm/sec is $\lesssim 10$ Å^2 which, for a helium-atom density of 2.2×10^{11} cm^{-3} ($p = 7\times10^{-6}$ Torr), yields a collision interval $t_Q \gtrsim 14$ msec.

Inasmuch as the collision intervals for the three relaxation processes are all considerably larger than the 4-msec storage time, we assume that the velocity distribution remains essentially the initial one and take $\langle v^{1/2}\rangle^2 = \langle v^2\rangle^{1/2}$ and assign a 50% uncertainty to account for the high degree of approximation. Thus we estimate $\langle v^{1/2}\rangle^2 = (3.3\pm1.7)\times10^5$ cm/sec.

Figure 7 shows a plot of the measured values of R vs $\alpha^{1/2}$ for the targets He, Ar, Kr, Xe, and CCl_4. (CCl_4 is essentially spherical; its lowest-order multipole moment is the octupole.) Values of α were taken from Rothe and Bernstein.[20] One sees that the values fall well along a straight line. The line through the experimental points is a least-squares fit of $R = k\alpha^{1/2}$ which gave $k = 4.14\times10^3$ cm$^{3/2}$ sec^{-1}. The two dashed lines indicate the range of values obtained from Eq. (15) corresponding to the uncertainty in $\langle v^{1/2}\rangle$. In the figure we include for comparison values of the momentum transfer rate constant calculated from Eq. (17).

Kocher, Clendenin, and Novick[21] in their time-of-flight work on the free lifetime of $He^+(2S)$ report a value of $\sigma \simeq 10\pi a_0^2 = 8.8\times10^{-16}$ cm^2 for the total deexcitation cross section of 15-eV ions on helium. This corresponds to a rate constant of $\simeq 2.4\times10^{-9}$ cm^3 sec^{-1}. A $v^{1/2}$ scaling of our result would predict $R = 4.7\times10^{-9}$ cm^3 sec^{-1} at 15 eV.

Lipworth and Novick[17] give the results of calculations of the cross sections σ_r for induced Lyman-α decay and σ_i for Penning ionization of He by $He^+(2S)$ ions with a mean velocity of 1.05×10^5 cm/sec. Their values are $\sigma_r = 34.4\pi a_0^2 = 3.03\times10^{-15}$ cm^2 and $\sigma_i = 15.9\pi a_0^2 = 1.40\times10^{-15}$ cm^2, yielding a total cross section of $4.43\times10^{-15} = 44.3$ Å^2. This is quite close to the value of $\sigma_{\rm eff}$ listed in Table I for He although our estimated relative velocity is more than three times the value used by Lipworth and Novick in their calculation.

TABLE II. Comparison of measured deexcitation rate constants R with polarization R_p, dipole R_d, and quadrupole R_q, constants. $\bar{\alpha}$, d, and q are the mean polarizability, dipole moment, and quadrupole moment used in calculating R_p, R_d, and R_q.

Target	$\bar{\alpha}$ [a] (Å^3)	d [b] (10^{-18} esu/cm)	q [b] (10^{-26} esu/cm^2)	R [c]	R_p	R_d [d]	R_q [d]
					(10^{-9} cm^3 sec^{-1})		
H_2	0.806	0.0	0.651	3.68(67)	3.7	0.0	2.4
N_2	1.74	0.0	−1.52	5.51(55)	5.5	0.0	4.2
O_2	1.57	0.0	−0.39	6.07(61)	5.2	0.0	1.7
CO_2	2.59	0.0	−4.3	11.3(16)	6.7	0.0	8.3
H_2O	1.45	1.84	1.0	18.5(19)	5.0	39.6	3.1
NH_3	2.16	1.47	1.0	20.9(21)	6.1	31.5	3.1

[a] Reference 17.
[b] Reference 21.
[c] See Table I.
[d] Using method of SMS (Ref. 8).

B. Molecular targets

In the case of impact on molecules one expects both the polarization and the molecular multipole fields to contribute to the Lyman-α deexcitation rate. For the linear symmetric molecules H_2, N_2, O_2, and CO_2 the lowest-order nonvanishing multipole moment is the quadrupole. The polarization field will in general be the sum of two dipole fields arising from induced moments $e\alpha_{\parallel}\cos\theta/r^2$ and $e\alpha_{\perp}\sin\theta/r^2$ where θ is the angle between the molecular axis and the line between the collision partners; $\alpha_{\parallel}$ and $\alpha_{\perp}$ are the polarizabilities for fields oriented parallel and perpendicular to the molecular axis. A calculation, then, requires the net electric field averaged over all molecular orientations. We do not carry out such a program here but have calculated the polarization and quadrupole-field deexcitation rates as if they were acting separately. Because the two fields are not everywhere parallel, the net effect is not simply the sum of the two, but should lie between the sum and the absolute value of the difference. The polarization-field deexcitation rate R_p was calculated using the constant determined from the measurements on the spherical targets together with the mean polarizabilities $\bar{\alpha} = \frac{1}{3}(2\alpha_{\perp} + \alpha_{\parallel})$. The quadrupole-field deexcitation rate was calculated using the relation $R_q = \sigma_q v$ ($v = 3.3\times10^5$ cm/sec), and

$$\sigma_q = 4.206(e\mu q/\hbar v)^{2/3}\ , \tag{18}$$

from the work of Slocomb, Miller, and Schaeffer (SMS); q is the molecular quadrupole moment. The values used for q are those recommended by Stogryn and Stogryn.[22] Table II contains the results of these calculations.[23] One sees that the sizes of the two effects are comparable; it is probably accidental that the polarization rate is in agreement with the experimental rates for H_2 and N_2 and nearly so for O_2. The case of CO_2 more clearly may require the existence of both mechanisms.

Kocher, Clendenin, and Novick[21] have also reported a value of $\sigma = 50\pi a_0^2 = 4.49\times10^{-15}$ cm^2 for the total deexcitation cross section for 15-eV $He^+(2S)$ on N_2. This corresponds to a rate of 11.8×10^{-9} cm^3 sec^{-1}.

Water and ammonia have large dipole fields which yield a rate constant according to SMS of

$$R_d = 5.924(e\mu d/\hbar)\ . \tag{19}$$

Values of R_p, R_d, and R_q are included in Table II for these targets also. Not included is a rate constant of $\simeq 0.60\times10^{-9}$ cm^3 sec^{-1} for both water and ammonia owing to an estimated effective octupole moment of $\simeq 10^{-34}$ esu cm^3. The experimental values of the total deexcitation rate constants for H_2O and NH_3 are about 50% less than the R_d values. This may reflect partial cancellation of the dipole field by the polarization and higher-order multipole fields. In any case for all the molecular targets, the measured values await a complete calculation of the Lyman-α deexcitation cross section before a more meaningful comparison can be made.

Finally, regarding the importance of Penning ionization we point out that consideration of the theory of ion-atom orbiting collisions (see Ref. 15, p. 477 and Ref. 19) together with the small size of $He^+(2S)$ in relation to the critical-orbiting impact parameter indicates that the Penning-ionization rate constant may be about equal to the momentum transfer rate constant. One sees that reduction of the measured total rate constants in Fig. 7 by the momentum transfer values (triangles) gives net values in better agreement with the sudden-approximation calculation (dashed lines).

In conclusion we believe that our measurements provide information regarding the collisional deexcitation of $He^+(2S)$ ions that would be difficult to achieve by other means. In particular, although our energy resolution is poor, it is doubtful that an ion-beam method could do better at the low-impact energy present in our experiments.

---

*Work supported by the U.S. Atomic Energy Commission.

[1]R. S. Kass and W. L. Williams, Phys. Rev. A 7, 10 (1973).

[2]S. J. Czuchlewski and S. R. Ryan, Bull. Am. Phys. Soc. 17, 1136 (1972); 18, 687 (1973); S. J. Czuchlewski, Ph.D. thesis (Yale University, 1973) (unpublished).

[3]F. J. Comes and U. Wenning, Z. Naturforsch. A 24, 587 (1969); Chem. Phys. Lett. 5, 199 (1970).

[4]W. L. Fite, R. T. Brackmann, D. G. Hummer, and R. F. Stebbings, Phys. Rev. 116, 363 (1959); 124, 2051 (1961).

[5]W. L. Fite, W. E. Kauppila, and W. R. Ott, Phys. Rev. Lett. 20, 409 (1968); W. R. Ott, W. E. Kauppila, and W. L. Fite, Phys. Rev. A 1, 1089 (1970).

[6]F. W. Byron, Jr. and J. I. Gersten, Phys. Rev. A 3, 620 (1971); Phys. Rev. Lett. 30, 115 (1973).

[7]J. I. Gersten, J. Chem. Phys. 51, 637 (1969).

[8]C. A. Slocomb, W. H. Miller, and H. F. Schaefer III, J. Chem. Phys. 55, 926 (1971).

[9]M. H. Prior, Phys. Rev. Lett. 29, 611 (1972).

[10]J. Shapiro and G. Breit, Phys. Rev. 113, 179 (1959); S. Klarsfeld, Phys. Lett. A 30, 382 (1969).

[11]H. A. Bethe and E. E. Salpeter, *Quantum Mechanics of One- and Two-Electron Atoms* (Academic, New York, 1957), Chap. 4, p. 285.

[12]L. Spitzer and J. L. Greenstein, Astrophys. J. 114, 407

(1951).
[13]E. E. Ferguson, F. C. Fehsenfeld, D. B. Dunkin, A. L. Schmeltekopf, and H. I. Schiff, Planet. Space Sci. 12, 1169 (1964).
[14]J. Sayers and D. Smith, in *Atomic Collision Processes*, edited by M. R. C. McDowell (North-Holland, Amsterdam, 1964), p. 871.
[15]J. B. Hasted, *Physics of Atomic Collisions* (Butterworths, London, 1964), Chap. 2, p. 35.
[16]L. I. Schiff, *Quantum Mechanics*, 3rd ed. (McGraw-Hill, New York, 1968), Chap. 8, p. 292.
[17]E. Lipworth and R. Novick, Phys. Rev. 108, 1434 (1957).
[18]L. Spitzer, *Physics of Fully Ionized Gases* (Wiley-Interscience, New York, 1956).
[19]M. A. Eliason and J. O. Hirschfelder, J. Chem. Phys. 30, 1426 (1959); M. A. Eliason, D. E. Stogryn, and J. O. Hirschfelder, Proc. Natl. Acad. Sci. USA 42, 546 (1956).
[20]E. W. Rothe and R. B. Bernstein, J. Chem. Phys. 31, 1619 (1959).
[21]C. A. Kocher, J. E. Clendenin, and R. Novick, Phys. Rev. Lett. 29, 615 (1972).
[22]D. E. Stogryn and A. P. Stogryn, Mol. Phys. 11, 371 (1966).
[23]Values for R_d and R_q calculated with the formulas of Gersten (Ref. 7) would be larger by factors of $3^{1/2}$ and $3^{1/3}$, respectively.